Fully Vectorial Accelerating Diffraction-Free Helmholtz Beams

Parinaz Aleahmad,[1] Mohammad-Ali Miri,[1] Matthew S. Mills,[1] Ido Kaminer,[2]
Mordechai Segev,[2] and Demetrios N. Christodoulides[1,*]

[1]*CREOL/College of Optics, University of Central Florida, Orlando, Florida 32816, USA*
[2]*Physics Department and Solid State Institute, Technion-Israel Institute of Technology, Haifa 32000, Israel*

(Received 2 October 2012; published 15 November 2012)

We show that new families of diffraction-free nonparaxial accelerating optical beams can be generated by considering the symmetries of the underlying vectorial Helmholtz equation. Both two-dimensional transverse electric and magnetic accelerating wave fronts are possible, capable of moving along elliptic trajectories. Experimental results corroborate these predictions when these waves are launched from either the major or minor axis of the ellipse. In addition, three-dimensional spherical nondiffracting field configurations are presented along with their evolution dynamics. Finally, fully vectorial self-similar accelerating optical wave solutions are obtained via oblate-prolate spheroidal wave functions. In all occasions, these effects are illustrated via pertinent examples.

DOI: 10.1103/PhysRevLett.109.203902 PACS numbers: 42.25.Fx, 03.50.De, 41.20.Jb

Since the prediction and experimental observation of optical Airy beams [1], there has been a flurry of activities in understanding and utilizing accelerating nondiffracting wave fronts [2–10]. As first indicated within the context of quantum mechanics [11], Airy wave packets tend to accelerate even in the absence of any external forces—a property arising from the inertial character of free-falling systems in a gravitational environment [12]. Interestingly, Airy waves represent the only possible self-similar accelerating solution to the free-particle Shrödinger equation when considered in one dimension. In optics, this peculiar class of waves is possible under paraxial diffraction conditions provided that they are truncated so as to have a finite norm [1]. In this realm, the intensity features of Airy beams propagate on a parabolic trajectory and exhibit self-healing properties, desirable attributes in a variety of physical settings [2]. In the last few years, such accelerating beams have been utilized in inducing curved plasma filaments [13], synthesizing versatile bullets of light [14], carrying out autofocusing and supercontinuum experiments [15], as well as manipulating microparticles [2]. The one-dimensional nature of these solutions was also successfully exploited in plasmonics [16–19]. Interestingly, shape-preserving accelerating beams can also be found in nonlinear settings, with Kerr, saturable, quadratic, and nonlocal nonlinearities [20–22]. In principle accelerating beams can also be generated though caustics [6,7]. Yet, such wave fronts are by nature not self-similar and thus cannot propagate over a long distance, a necessary feature to reach large deflections.

Until recently, it was generally believed that shape-preserving accelerating beams belong exclusively to the domain of Shrödinger-type equations [11], which for general waves (e.g., electromagnetic, acoustic, etc.) will only be valid under paraxial conditions. Quite recently, however, nonparaxial, shape-preserving accelerating beams in the form of higher-order Bessel functions have been found as solutions of Maxwell equations [23] and experimentally demonstrated [24,25]. This new family of waves represents exact vectorial solutions to the two-dimensional Helmholtz equation, and as such they follow circular trajectories (on a quadrant) on which the magnitude of acceleration is constant. Unlike paraxial Airy beams, these nonparaxial waves can in principle intersect the propagation axis at 90°, thus considerably expanding their bending horizon. Such behavior can be particularly useful in many and diverse applications such as in nanophotonics where nonparaxiality is absolutely necessary. Apart from optics, these solutions can be similarly realized in other electromagnetic frequency bands as well as in acoustics. Given that Airy beams are unique within 1D paraxial optics, the question naturally arises if the aforementioned higher-order Bessel accelerating diffraction-free waves represent the only possible solution. In other words, are there any other vectorial solutions to the full-Maxwell equations that could in general accelerate along more involved trajectories? If so, can they be extended in the three-dimensional vectorial regime, and are they again self-healing in character?

In this Letter, we show that indeed other families of accelerating nondiffracting wave solutions to Maxwell's equations also exist. By utilizing the underlying symmetries of the corresponding Helmholtz problem, we demonstrate both theoretically and experimentally self-healing vectorial wave fronts—capable of following elliptic trajectories and hence experiencing a nonuniform acceleration. The existence of such beams clearly indicates that shape preservation is not an absolute must in attaining accelerating diffraction-free propagation. In addition, we theoretically explore the dynamics of self-similar accelerating 3D vectorial spherical wave functions along with their power flow characteristics. Other solutions of such classes of 3D accelerating ring wave fronts are also obtained via

oblate-prolate spheroidal wave functions. Our results may pave the way toward synthesizing more general classes of accelerating waves for applications in optics and ultrasonics.

We begin our analysis by first considering the Helmholtz equation in two dimensions $(\partial_{xx} + \partial_{yy} + k^2)\{\vec{E}, \vec{H}\} = 0$, that governs both the electric and magnetic field components of an optical wave. For the transverse-electric (TE) case, the electric field involves only one component, i.e., $\vec{E} = E_z(x, y)\hat{z}$ from where the magnetic vectors H_x, H_y can be readily deduced from Maxwell's equations for a given wave number $k = \omega n/c$. By introducing elliptic coordinates, the Helmholtz problem takes the form

$$\left[\frac{2}{f^2(\cosh 2u - \cos 2v)}\left(\frac{\partial^2}{\partial u^2} + \frac{\partial^2}{\partial v^2}\right) + k^2\right]E_z = 0, \quad (1)$$

where $x = f\cosh u \cos v$, $y = f\sinh u \sin v$ with $u \in [0, \infty)$, and $v \in [0, 2\pi)$. In this representation, f represents a semifocal distance and is associated with the ellipticity of the system. Equation (1) is in turn solved via standard separation of variables, e.g., $E_z = R(u)S(v)$ in which case one obtains the following ordinary differential equations:

$$\left[\frac{d^2}{dv^2} + (a - 2q\cos 2v)\right]S(v) = 0, \quad (2a)$$

$$\left[\frac{d^2}{du^2} - (a - 2q\cosh 2u)\right]R(u) = 0, \quad (2b)$$

with the dimensionless quantity $q = f^2k^2/4$. On the other hand, the parameter a in Eqs. (2) can be obtained from a sequence of eigenvalues $a_m (m = 1, 2, \ldots)$ corresponding to the Mathieu equation (2a). From this point on, both the angular $S_m(v)$ and radial $R_m(u)$ Mathieu functions can be uniquely determined. A possible elliptic solution to these equations is expected to display a circulating power flow in the angular direction. This can be achieved through a linear superposition of the standard solutions to Eqs. (2) with constant real coefficients A and B [26],

$$E_z^m(u, v; q) = Ace_m(v; q)Mc_m^{(1)}(u; q) + iBse_m(v; q)Ms_m^{(1)}(u; q), \quad (3)$$

where ce_m and se_m represent even and odd angular Mathieu functions of order m while $Mc_m^{(1)}$ and $Ms_m^{(1)}$ stand for their corresponding radial counterparts (of the first kind). Figures 1(a) and 1(b) show a two-dimensional plot of these elliptic modes for two different values of q when $m = 8$ and $A = B = 1$. As one would expect, the ellipticity of the light trajectory increases with the semifocal parameter f. What is also clearly evident from Figs. 1(a) and 1(b) is the fact that the intensity of the rings does not remain constant in the angular domain. In other words, unlike other families of diffraction-free beams, these elliptical beams can propagate in an accelerating fashion up to 90° without exactly preserving their shape. Note that the power density, especially that of the first lobe, tends to increase along the major axis while it reaches its lowest value when it is passing the minor axis of the ellipse. Interestingly, this behavior persists even under dynamic conditions, i.e., when such a field configuration is launched on axis. Given that all optical diffraction-free arrangements (including those mentioned here) possess, strictly speaking, an infinite norm, in practice they have to be apodized in order to be experimentally observed. Figure 1(c) depicts an elliptic trajectory when a weakly truncated (using a Gaussian apodization) version of the field profile in Eq. (3) is used at $v = 0$, e.g., when launched from the major axis. These simulations are carried out for $\lambda = 1\ \mu$m, $m = 150$, and $f = 31.8\ \mu$m provided that the width of the first lobe is approximately 550 nm. In this case, the intensity $|E_z|^2$ of the main lobe follows an ellipse, starting at 34 μm and eventually reaching 12 μm, on the y axis. On the other hand, when this same beam is launched from the y axis [$v = \pi/2$, in Eq. (3)] the main lobe meets the major axis at 34 μm [Fig. 1(d)]. Unlike the previously reported Bessel wave fronts propagating on circular trajectories [23], these beams can exhibit diffraction-free behavior in spite of the fact that their intensity features are no longer invariant during propagation because of their varying acceleration. Figure 1(d) also indicates that the intensity of the lobes tends to eventually increase before intersecting the x axis. Conversely, it decreases when

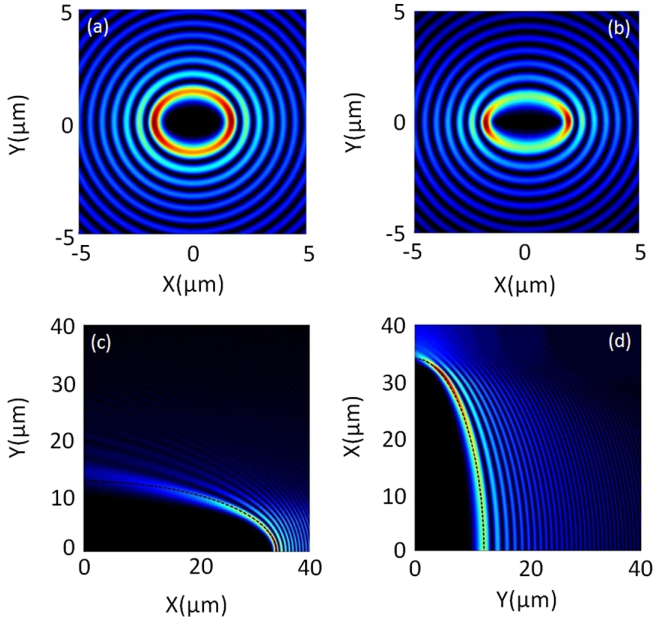

FIG. 1 (color online). Intensity profiles of elliptic modes of order $m = 8$ when (a) $q = 10$ and (b) $q = 20$. (c) Propagation pattern of a weakly truncated Mathieu beam when it is launched from the major axis, when $m = 150$ and $q = 10^4$, starting from $x = 34\ \mu$m and reaching $y = 12\ \mu$m on the minor axis. (d) Same Mathieu beam as in (c), launched from the minor axis, starting at $y = 12\ \mu$m and reaching $x = 34\ \mu$m. In (d), note the increase in intensity at the apogee point.

reaching the y axis for the case shown in Fig. 1(c). Interestingly, this response is in agreement with the results of Figs. 1(a) and 1(b) when taken over the first quadrant. The variation of the intensity levels along these elliptic trajectories can be better understood from power conservation requirements. Given that in elliptic coordinates, a given lobe moves on a $u = \text{const}$ trajectory, then, as u increases (needed for establishing a broad wave front), the encompassing region becomes almost circular. As a result, this same power flow happens to be constricted when crossing the major axis, hence elevating the intensity levels within the beam. Conversely, the intensity drops in the other regime [Fig. 1(c)]. To demonstrate that these beams remain actually diffraction-free, we next examine their self-healing properties. Figure 2(a) depicts the propagation dynamics of such a Mathieu wave front when its main lobe is initially obstructed [Fig. 2(b)]. The parameters used are the same as those of Fig. 1(c). The self-healing mechanism is here clearly evident after propagating a distance of 5 μm.

In our experiments, elliptic Mathieu beams were generated in the Fourier domain by appropriately imposing a phase function through a spatial light modulator. In this setup a broad Gaussian beam from a continuous-wave $\lambda = 633$ nm laser source was used. The resulting phase-modulated wave was then demagnified and projected onto the back focal plane of a 60× objective lens in order to produce the Mathieu function in the spatial domain. Subsequently the evolution of this beam was monitored along the propagation direction using a 60× objective lens and a CCD camera. Figure 3(a) depicts experimental results associated with the intensity profile of a Mathieu elliptic beam when $m = 1400$ and $q = 2.5 \times 10^5$. In this case, the phase mask was judiciously designed so as to launch this elliptic beam toward the major axis (where apogee was reached) under the constraint of a limited numerical aperture (~ 0.7), arising from the first lens in the system. This beam was found to intersect again the horizontal launching line after 200 μm. Conversely, when this same beam was launched in a complementary fashion, its apogee was attained on the minor axis, Fig. 3(b). In both cases the elliptic trajectory is clearly apparent. The fact that the intensity of this elliptic beam is maximum on the major axis is also evident, in accord with theoretical predictions [Fig. 1(d)]. These results are in good agreement with their corresponding simulations presented in Figs. 3(c) and 3(d).

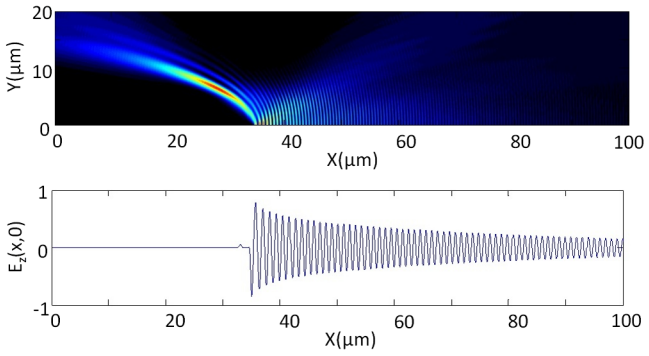

FIG. 2 (color online). (a) Self-healing property of a truncated Mathieu beam (b), when it is launched from the major axis, with $m = 150$, $q = 10^4$, and with its main lobe initially truncated.

Apart from the aforementioned two-dimensional accelerating diffraction-free solutions, other more involved three-dimensional accelerating field configurations also exist. To demonstrate this possibility, we consider the Helmholtz equation in its more general form. To treat this problem we introduce auxiliary magnetic and electric vector potentials, $\mathbf{A}$ and $\mathbf{F}$, through which one can recover the electrodynamic field components [27], i.e.,

$$\mathbf{E} = -\nabla \times \mathbf{F} - \frac{1}{i\omega\epsilon}\nabla \times \nabla \times \mathbf{A},$$
$$\mathbf{H} = \nabla \times \mathbf{A} - \frac{1}{i\omega\mu}\nabla \times \nabla \times \mathbf{F}. \tag{4}$$

By employing a proper Lorentz gauge along with their respective scalar potentials, one arrives at a vectorial Helmholtz equation for the vector potentials, $\nabla^2\{\mathbf{A}, \mathbf{F}\} + k^2\{\mathbf{A}, \mathbf{F}\} = 0$. Pertinent solutions to the underlying Maxwell equations can be obtained by separately considering transverse electric and transverse magnetic field arrangements. For example if we set $\mathbf{A} = 0$, $\mathbf{F} = \hat{y}\psi$, this leads to a transverse electric solution with respect to y, i.e., $E_y = 0$. On the other hand, if $\mathbf{A} = \hat{y}\psi$, $\mathbf{F} = 0$, a transverse magnetic field mode is established with respect to y, implying that the y component of magnetic field is now zero. In both cases the scalar function ψ satisfies $\nabla^2\psi + k^2\psi = 0$.

In spherical coordinates, this latter scalar Helmholtz problem can be directly solved. More specifically, we find

$$\psi(x, y, z) = j_n(kr)P_n^m(\cos\theta)e^{im\phi}, \tag{5}$$

where $j_n(x)$ represents spherical Bessel functions of the first kind, of order n, $P_n^m(x)$ stands for associated Legendre

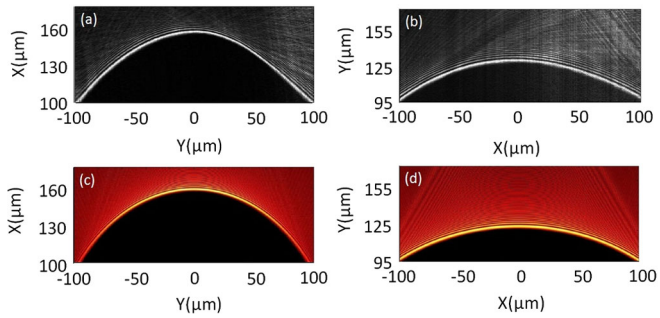

FIG. 3 (color online). Observed intensity profile of an elliptic Mathieu beam with $m = 1400$ and $q = 2.5 \times 10^5$ when propagating (a) toward the major axis and (b) minor axis. (c), (d) Corresponding theoretical simulations for the experimental results in (a),(b).

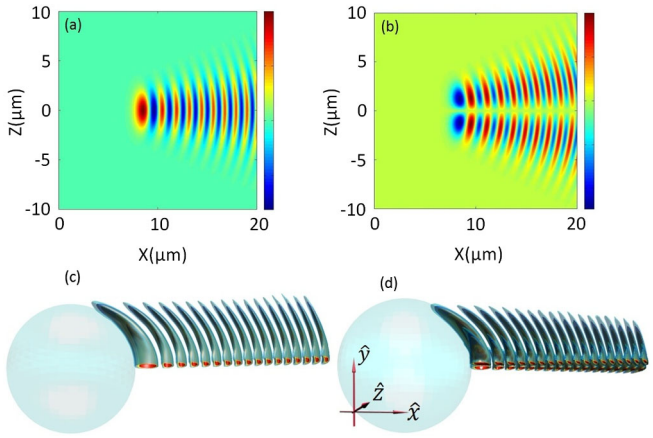

FIG. 4 (color online). Two-dimensional cross section of the TE mode electric vector potential **F** associated with spherical coordinates when (a) $m = n = 50$ and (b) $n = 50$; $m = 49$. (c), (d) Accelerating diffraction-free dynamics when an apodized beam in (a),(b) is launched in the x-z plane.

polynomials of degree n with $-n \leq m \leq n$, and k denotes the free space wave number. From here, $\{\mathbf{E}, \mathbf{H}\}$ can be deduced from Eqs. (4) depending on whether the mode is TE or TM. Figures 4(a) and 4(b) show two-dimensional profiles of the electric vector potential **F** associated with a TE field configuration when $m = n = 50$ and $n = 50$, $m = 49$, respectively. The corresponding diffraction-free dynamics resulting from apodized versions of these beams are shown in Figs. 4(c) and 4(d) when launched in the x-z plane. These five-component vectorial waves propagate in a self-similar fashion within the first quadrant of the x-y plane, by revolving around the z axis. The TM case can be similarly analyzed.

Additional families of three-dimensional accelerating solutions also exist in other coordinate systems. For example, by adopting prolate spheroidal coordinates (ξ, η, ϕ), the scalar function ψ can be determined and is given by $\psi = R_{mn}(\xi, \gamma)S_{mn}(\eta, \gamma)e^{im\phi}$ where $\gamma = fk/2$ with f being the semifocal distance in this system. In the last equation, R_{mn}, S_{mn} represent radial and angular prolate spheroidal wave functions of orders m, n. Figure 5(a) provides a two-dimensional plot of the electric vector potential **F** associated with a TE accelerating mode, within the x-z plane. The dynamical evolution of this beam (after a Gaussian apodization) is depicted in Fig. 5(b). The self-similar behavior of this field distribution is again evident. Similarly, accelerating solutions in oblate spheroidal coordinates can also be found under TE or TM conditions.

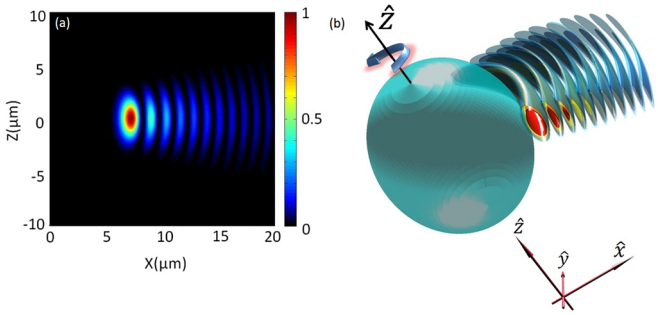

FIG. 5 (color online). (a) Two-dimensional profile associated with the electric vector potential **F** in prolate spheroidal coordinates when $m = n = 30$ and $\gamma = 20$. (b) Dynamical evolution of this beam when launched in the x-z plane.

In conclusion we have demonstrated that Maxwell's equations can admit three-dimensional fully vectorial accelerating beams. One such class of solutions was found to follow elliptic trajectories and hence experiencing a nonuniform acceleration, in spite of the fact that the corresponding intensity features do not remain invariant during propagation. Experimental observations of these elliptically accelerating beams were reported, corroborating our predictions. Other 3D families of accelerating wave fronts were also theoretically explored including TE or TM spherical and spheroidal wave functions. Our results may be of importance in physical settings where vectorial nonparaxiality is required. These features could be potentially useful in nanophotonics, plasmonics, microparticle manipulation, and ultrasonics, to mention a few.

This work was supported by the Air Force Office of Scientific Research (MURI Grant No. FA9550-10-1-0561).

*Corresponding author.
demetri@creol.ucf.edu

[1] G. A. Siviloglou and D. N. Christodoulides, Opt. Lett. **32**, 979 (2007); G. A. Siviloglou, J. Broky, A. Dogariu, and D. N. Christodoulides, Phys. Rev. Lett. **99**, 213901 (2007).
[2] J. Baumgartl, M. Mazilu, and K. Dholakia, Nature Photon. **2**, 675 (2008).
[3] T. Ellenbogen, N. Voloch-Bloch, A. Ganany-Padowicz, and A. Arie, Nature Photon. **3**, 395 (2009).
[4] G. Porat, I. Dolev, O. Barlev, and A. Arie, Opt. Lett. **36**, 4119 (2011).
[5] H. I. Sztul and R. R. Alfano, Opt. Express **16**, 9411 (2008).
[6] L. Froehly, F. Courvoisier, A. Mathis, M. Jacquot, L. Furfaro, R. Giust, P. A. Lacourt, and J. M. Dudley, Opt. Express **19**, 16455 (2011).
[7] E. Greenfield, M. Segev, W. Walasik, and O. Raz, Phys. Rev. Lett. **106**, 213902 (2011).
[8] I. Dolev, T. Ellenbogen, and A. Arie, Opt. Lett. **35**, 1581 (2010).
[9] I. M. Besieris and A. M. Shaarawi, Phys. Rev. E **78**, 046605 (2008).
[10] N. K. Efremidis, Opt. Lett. **36**, 3006 (2011).
[11] M. V. Berry and N. L. Balazs, Am. J. Phys. **47**, 264 (1979).
[12] D. M. Greenberger, Am. J. Phys. **48**, 256 (1980).
[13] P. Polynkin, M. Koleskik, J. V. Moloney, G. A. Siviloglou, and D. N. Christodoulides, Science **324**, 229 (2009).
[14] A. Chong, W. H. Renninger, D. N. Christodoulides, and F. W. Wise, Nature Photon. **4**, 103 (2010).
[15] C. Ament, P. Polynkin, and J. V. Moloney, Phys. Rev. Lett. **107**, 243901 (2011).

[16] A. Salandrino and D. N. Christodoulides, Opt. Lett. **35**, 2082 (2010).
[17] L. Li, T. Li, S. M. Wang, C. Zhang, and S. N. Zhu, Phys. Rev. Lett. **107**, 126804 (2011).
[18] A. Minovich, A. E. Klein, N. Janunts, T. Pertsch, D. N. Neshev, and Y. S. Kivshar, Phys. Rev. Lett. **107**, 116802 (2011).
[19] P. Zhang, S. Wang, Y. Liu, X. Yin, C. Lu, Z. Chen, and X. Zhang, Opt. Lett. **36**, 3191 (2011).
[20] I. Kaminer, M. Segev, and D. N. Christodoulides, Phys. Rev. Lett. **106**, 213903 (2011).
[21] I. Dolev, I. Kaminer, A. Shapira, M. Segev, and A. Arie, Phys. Rev. Lett. **108**, 113903 (2012).
[22] R. Bekenstein and M. Segev, Opt. Express **19**, 23706 (2011).
[23] I. Kaminer, R. Bekenstein, J. Nemirovsky, and M. Segev, Phys. Rev. Lett. **108**, 163901 (2012).
[24] P. Zhang, Y. Hu, D. Cannan, A. Salandrino, T. Li, R. Morandotti, X. Zhang, and Z. Chen, Opt. Lett. **37**, 2820 (2012).
[25] F. Courvoisier, A. Mathis, L. Froehly, R. Giust, L. Furfaro, P. A. Lacourt, M. Jacquot, and J. M. Dudley, Opt. Lett. **37**, 1736 (2012).
[26] M. Abramowitz and I. Stegun, *Handbook of Mathematical Functions* (Dover, New York, 1972).
[27] R. F. Harrington, *Time-Harmonic Electromagnetic Fields* (Wiley-IEEE, New York, 2001).